Journal of Power Sources 216 (2012) 28–32

Contents lists available at SciVerse ScienceDirect

Journal of Power Sources

journal homepage: www.elsevier.com/locate/jpowsour

Enhanced electrocatalytic performance of Pt monolayer on nanoporous PdCu alloy for oxygen reduction

Linxi Hou [a], Huajun Qiu [b,*]

[a] School of Materials Science and Chemical Engineering, Ningbo University, Ningbo 315211, China
[b] School of Chemistry and Chemical Engineering, Shandong University, Jinan 250100, China

HIGHLIGHTS

- Pt monolayer-covered nanoporous PdCu catalysts are prepared by a Cu-underpotential deposition–Pt displacement strategy.
- Compared with Pt/C catalyst, the Pt monolayer-modified nanoporous PdCu show much enhanced activity and stability for oxygen reduction reaction (ORR).
- Pt monolayer on PdCu alloy core with a Pd:Cu ratio of 1 shows the highest activity for ORR.

ARTICLE INFO

Article history:
Received 12 March 2012
Received in revised form
20 May 2012
Accepted 21 May 2012
Available online 29 May 2012

Keywords:
Dealloying
Electrocatalyst
Fuel cell

ABSTRACT

By selectively dealloying Al from $Pd_xCu_{20-x}Al_{80}$ ternary alloys in 1.0 M NaOH solution, nanoporous PdCu (np-PdCu) alloys with different Pd:Cu ratios are obtained. By a mild electrochemical dealloying treatment, the np-PdCu alloys are facilely converted into np-PdCu near-surface alloys with a nearly pure-Pd surface and PdCu alloy core. The np-PdCu near-surface alloys are then used as substrates to fabricate core–shell catalysts with a Pt monolayer as shell and np-PdCu as core by a Cu-underpotential deposition–Pt displacement strategy. Electrochemical measurements demonstrate that the Pt monolayer on np-Pd_1Cu_1 (Pt/np-Pd_1Cu_1) exhibits the highest Pt surface-specific activity towards oxygen reduction, which is ~5.8-fold that of state-of-the-art Pt/C catalyst. The Pt/np-Pd_1Cu_1 also shows much enhanced stability with ~78% active surface retained after 10,000 cycles (0.6–1.2 V vs. RHE). Under the same condition, the active surface of Pt/C drops to ~28%.

1. Introduction

Hydrogen-based polymer electrolyte fuel cells (PEMFCs) have raised great interest due to the demand for low-cost and renewable energy in various fields [1–3]. As a promising future technology, however, the commercial application of PEMFCs is limited by the inherently slow oxygen reduction kinetics and a corresponding overpotential of the cathodic half cell [1–4]. Although much research has been made to develop non-Pt catalysts in recent years, Pt-based catalysts still represent the highest oxygen reduction reaction (ORR) activity. Currently, the state-of-the-art commercial ORR catalyst is fine Pt nanoparticles (~3 nm) dispersed on carbon supports (Pt/C). However, the overpotential on Pt/C cathode is still high and its mass activity is still far from satisfactory. Moreover, due to the corrosion of the carbon support and the weak interaction between catalyst and support, the Pt nanoparticles usually undergo aggregation and Oswald ripening which would induce much loss of the electrochemical active surface area (EASA) during long-term operation [5].

Recent efforts in ORR electrocatalysis have focused on improving both the catalytic activity and utilization of precious Pt by preparing Pt-based alloy [6–16] and core–shell [17–23] nanostructures. For example, the monolayer Pt shell supported on other metal cores shows significantly enhanced activity than commercial Pt/C due to the synergistic effect from the core [18]. The activity of the Pt monolayer depends strongly on the electronic and structural properties of the core [24,25]. Thus, further enhancing the catalytic activity and stability of the Pt monolayer by optimizing the core is of considerable interest. Pt monolayer on a Pd core has been demonstrated to exhibit a higher activity for ORR compared with Pt monolayer on other metal cores such as Au, Ru, Rh, and Ir [24]. Since Pd is also a precious metal, lowering Pd content in the core is also quite necessary. Using Pd-based alloys (such as PdCu alloy) as cores should be an effective way to lower Pd content. More

* Corresponding author. Tel.: +86 532 80662760; fax: +86 532 80662778.
E-mail address: qiuhuajun@gmail.com (H. Qiu).

0378-7753/$ – see front matter © 2012 Elsevier B.V. All rights reserved.
doi:10.1016/j.jpowsour.2012.05.064

importantly, it has been reported that the presence of a non-precious metal (Cu or Fe) in the Pd-based core can further enhance the activity and stability of the Pt monolayer shell [17].

On the other hand, while most research has focused on improving the performance of Pt/C-like nanoparticle-based supported catalysts [26–30], more recently supportless Pt nanostructures were reported to exhibit enhanced stability with less EASA loss during long-term operation [31–33]. For example, supportless Pt nanotubes, free-standing multi-armed Pt nanowires, etc. have shown improved activity and durability for ORR compared with Pt/C [31,32]. However, it is noted that most of these catalysts show little mass-specific activity enhancement compared with Pt/C mostly due to their low utilization of Pt. It is thus highly desirable to fabricate new nanocatalysts of practical value which exhibit high catalytic activity, durability, and noble metal utilization.

Dealloying (i.e., selective dissolution of active species from an alloy) has been demonstrated to be very powerful in generating free-standing three-dimensional (3D) nanoporous metals [34–36]. Unlike traditional nanoparticle-based electrocatalysts, nanoporous metals obtained by dealloying hold a unique combination of a highly conductive network and a highly accessible open nanoporosity, which is particularly favorable for electrocatalysis [35–38]. In this work, an interesting type of supportless nanoporous PdCu (np-PdCu) alloys obtained by dealloying PdCuAl ternary alloys are used as the cores for the fabrication of Pt monolayer on np-PdCu core–shell catalysts (Pt/np-PdCu) by Cu-underpotential deposition (UPD)–Pt displacement strategy [18,24,25]. By effectively avoiding the problems of nanoparticle aggregation and loss of contact to carbon support involved in Pt/C-like catalysts, this novel nanoporous core–shell electrocatalyst shows greatly improved durability and activity towards ORR compared with Pt/C catalyst.

2. Experimental

$Pd_xCu_{20-x}Al_{80}$ (at.%, $x = 20$, 15, 10, and 6) alloy foils were made by refining pure (>99.9%) Pd, Cu and Al in an arc furnace, followed by melt-spinning under an argon-protected atmosphere [34]. np-Pd and np-PdCu with different Pd:Cu ratios were prepared by dealloying the alloy foils in 1 M NaOH solution at 70 °C. The Johnson-Matthey Pt/C (20 wt.%) catalyst was purchased from Alfa Aesar.

np-PdCu (2.0 mg) were dispersed with carbon powder (1.0 mg), isopropanol (300 μL), and Nafion solution (100 μL, 5 wt.%) by ultrasonic for 30 min. The obtained suspension (4 μL) was deposited on a glassy carbon electrode (4 mm in diameter) and dried. Considering that certain Cu atoms on np-PdCu surface were unstable, the np-PdCu electrodes were cycled from 0 to 1.35 V vs. RHE in 0.1 M $HClO_4$ solution until a steady state was reached (scan rate: 50 mV s^{-1}). The Cu monolayer-covered np-PdCu were prepared by 2 potential cycles from 0.37 to 0.90 V in 50 mM H_2SO_4 + 50 mM $CuSO_4$ solution (scan rate: 5 mV s^{-1}) [18]. The Cu monolayer-covered np-PdCu were then rinsed and immersed in 1.0 mM K_2PtCl_4 + 50 mM H_2SO_4 solution for 3 min to replace Cu with Pt. Electrochemical experiments were performed on a CHI 760C electrochemical workstation. A three-electrode system was used with a modified electrode as working electrode, a Pt foil as counter electrode, and a mercury sulfate electrode as reference electrode. All potentials were referred to RHE. The EASA of Pt is calculated according to the equation: EASA (cm^2) = Q_H/210 where Q_H (μC) is the charge associated with hydrogen underpotential deposition which is obtained by integrating the CV curve in 0.1 M $HClO_4$ between 0 and 0.4 V, and 210 (μC cm^{-2}) is the charge corresponding to the adsorption of a monolayer of hydrogen on a polycrystalline Pt surface. All samples were characterized on a Bruker D8 advanced X-ray diffractometer (XRD), a JEOL JSM-6700F field emission scanning electron microscope (SEM) equipped with an Oxford INCA X-sight energy dispersive X-ray spectrometer (EDS), and a JEM-2100 high-resolution transmission electron microscope (TEM).

3. Results and discussion

np-PdCu with different Pd:Cu ratios (Pd_3Cu_1, Pd_1Cu_1, and Pd_3Cu_7) were prepared by dealloying $Pd_xCu_{20-x}Al_{80}$ ternary alloys. This dealloying route can achieve a nearly 100% yield with essentially no loss of noble metals and the ratio of Pd:Cu in the resulting np-PdCu can be pre-determined by controlling the feed ratios of the ternary alloys during the alloy refining process. This is quite different to the metal ion-reduction approach where the feed ratio of metal salts does not guarantee the same composition in the alloy products due to the different reducing capacities of metal ions.

For the first dealloying in an alkaline solution (1 M NaOH), the ternary alloys were etched at 70 °C. At this high temperature, the dealloying rate is greatly improved compared with that at room temperature and ca. 5 h are needed for the complete removal of Al. At room temperature, ca. 24 h are needed for the complete removal of Al. After the dealloying in the alkaline solution, EDS analysis shows that Al can be completely removed and the contents of Pd and Cu are unchanged (data not shown). The removal of Al and formation of uniform np-PdCu alloy structure have also been further confirmed by XRD analysis which has been presented in our previous work [39].

Fig. 1 shows the SEM image of np-Pd_1Cu_1 obtained by dealloying of $Pd_{10}Cu_{10}Al_{80}$ in 1 M NaOH solution at 70 °C. It is observed that np-Pd_1Cu_1 has an open bicontinuous ligament–pore structure with a narrow ligament size distribution (3–6 nm). Herein, only the SEM image of np-Pd_1Cu_1 was shown as a representative. The detailed characterization of all four samples using both SEM and TEM can be found in previous work [39]. It should be mentioned that other np-PdCu alloys have the same nanoporous structure with similar ligament sizes of ~3–6 nm. It is known that under the same dealloying conditions, the surface diffusivity of adatom follows Pt < Pd < Au < Ag < Cu [34], and the faster the diffusivity is, the larger the metal ligament becomes. In the present case, np-PdCu alloys with uniform alloy ligaments of less than 10 nm are obtained despite the different Cu contents. This phenomenon can be attributed to a so-called “pinning effect” of Pd adatoms with a low diffusivity on the diffusion of Cu adatoms during the dealloying, resulting in the formation of ultrafine PdCu alloy ligaments when the H_2 bubbling just stops. Since np-Pd_3Cu_7 contains more Cu atoms with a higher diffusivity, the ligaments of this sample coarsen more quickly compared with those of the other samples when extending the dealloying time (figures not shown).

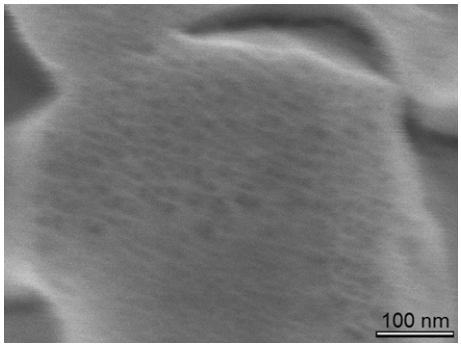

Fig. 1. SEM image of np-Pd_1Cu_1.

Before the Cu-UPD, np-PdCu were further electrochemically dealloyed by potential cycling (−0.05–1.35 V) to form a nearly pure-Pd surface. Fig. 2a shows the change of cyclic voltammograms (CVs) of np-Pd_3Cu_7 (as the representative) with increasing scan cycles in 0.1 M $HClO_4$ solution. In the first scan, the big anodic peak noticed between 0.3 and 0.8 V is due to the leaching of exposed Cu atoms on alloy surface [40]. The large current response between 0.8 and 1.3 V can be ascribed to further dissolution of Cu at high potentials [6]. The current from Cu dissolution decreases quickly with increasing scan cycles and disappears after ∼30 cycles. Meanwhile, the peak for oxide reduction at ∼0.75 V shifts positively and the peaks for hydrogen adsorption/desorption between −0.05 and 0.3 V increase. Finally, the CV of np-Pd_3Cu_7 is basically the same as that of np-Pd and changes negligibly with further scan, indicating the formation of a nearly pure-Pd shell by the mild electrochemical dealloying. EDS analysis shows that after the electrochemical dealloying, the Cu content in np-Pd_3Cu_7 only slightly decreases (from ∼70 at.% to ∼67 at.%), indicating that the dealloying of Cu only occurs on the surface sites and the large amount of Cu should exist in deeper layers. It should be mentioned that quite similar electrochemical surface dealloying process also occurred on np-Pd_3Cu_1 and np-Pd_1Cu_1 (with relatively lower currents from Cu dissolution), which have been reported in previous work.[39] The np-PdCu with a nearly pure-Pd shell and PdCu alloy core is usually called near-surface alloy. Since the dealloying only occurs on the surface (maybe one or two atomic layers), XRD analysis shows that the positions of the three diffraction peaks from the electrochemically dealloyed np-Pd_1Cu_1 (i.e., np-Pd_1Cu_1 near-surface alloy) are almost the same as those from original np-Pd_1Cu_1 and no diffraction peaks related to pure-Pd appear (Fig. 2b). It is worth mentioning that the electrochemical dealloyed np-PdCu has the same ligament/pore structure with ligament size of 3–6 nm as the original np-PdCu (figures not shown). For the structure stability test, we put these np-PdCu near-surface alloys back to the NaOH dealloying solution. It is observed that the np-Pd_3Cu_7 near-surface alloy with a nearly pure-Pd shell becomes much more resistant to coarsening than the pristine np-Pd_3Cu_7. After 24 h incubation in the dealloying solution at room temperature, no obvious coarsening of the ligaments is observed.

Fig. 3 shows the CV for Cu-UPD on the np-Pd_1Cu_1 near-surface alloy. The amount of Pt deposited is calculated based on the Cu-UPD charge: $Mass_{Pt}\,(mg) = [Q/(2 \times 96{,}485)] \times 195$, where Q (mC) is the total charge for Cu-UPD, 2 is number of electrons associated with UPD for a Cu atom, 96,458 (C mol^{-1}) is Faraday's constant and 195 (g mol^{-1}) is the molar mass of Pt. The calculated wt.% of Pt in the Pt/np-$Pd_1Cu_1$is 15.3%, which is in agreement with the value obtained by EDS analysis (Fig. 4b). After the deposition of a Pt monolayer on the np-PdCu near-surface alloy, electron microscopy

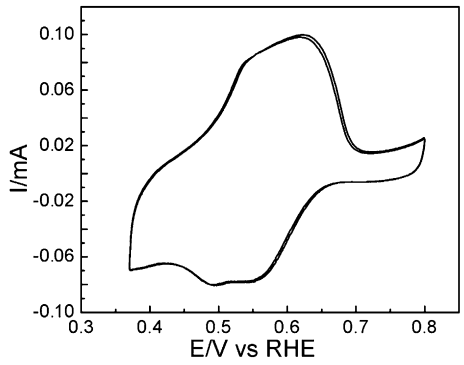

Fig. 3. CVs of np-Pd_1Cu_1 in 50 mM H_2SO_4 + 50 mM $CuSO_4$ solution, scan rate: 5 mV s^{-1}.

characterization (figure not shown) suggests that the Pt/np-PdCu inherits the bicontinuous ligament–pore structure of np-PdCu with the same ligament size of ∼3–6 nm, indicating that only monolayer Pt is deposited. The same phenomenon has also been observed from the np-Pd. EDS analysis confirms that the presence of Pt in the three Pt/np-PdCu with the ratio of Pd:Cu well-preserved (Fig. 4a and b). Due to the similar ligament sizes of the three Pt/np-PdCu, the at.% of loaded Pt on the three Pt/np-PdCu are almost the same. The at.% of Pd is 69.9%, 48.1% and 27.4% for Pt/np-Pd_3Cu_1, Pt/np-Pd_1Cu_1, and Pt/np-Pd_3Cu_7, respectively, which give the wt.% of Pd in the three samples (72.4% for Pt/np-Pd_3Cu_1, 55.0% for Pt/np-Pd_1Cu_1, and 34.3% for Pt/np-Pd_3Cu_7). These results clearly shows that the amounts of total noble metal loadings in the three samples follow the order that Pt/np-Pd_3Cu_1 > Pt/np-Pd_1Cu_1 > Pt/np-Pd_3Cu_7.

Fig. 5a shows the CVs of Pt/np-Pd_1Cu_1, Pt/np-Pd and Pt/C in 0.1 M $HClO_4$ solution. Compared with that of Pt/C, the oxide reduction peaks of Pt/np-Pd_1Cu_1 and Pt/np-Pd shift clearly to higher potentials by ∼50 mV. The positive potential shift can be attributed to the delay in the onset of Pt–OH formation, and implies an enhanced oxygen reduction activity [41]. Fig. 5b displays the ORR polarization curves of Pt/np-PdCu, Pt/np-Pd and Pt/C in O_2-saturated 0.1 M $HClO_4$ solution. All curves exhibit two distinguishable potential regions: a mixed kinetic-diffusion control region (0.8–1.0 V) and a well-defined diffusion controlled region (below 0.8 V). Although these samples have similar EASA, Pt/np-Pd_1Cu_1 exhibits a much higher half-wave potential at ∼0.92 which is about 60 mV more positive than that of Pt/C (∼0.86 V), indicating remarkably improved reaction kinetics for ORR. To probe the intrinsic activities of the Pt/np-PdCu, the kinetic currents at 0.90 V are normalized to the EASA (determined from the H_{ads} charge) and Pt mass (obtained by integrating the Cu-UPD charge). It is worth

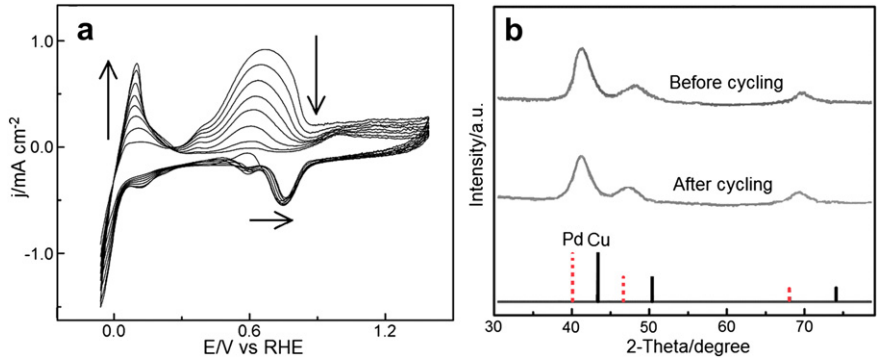

Fig. 2. CVs of np-Pd_3Cu_7 at different scan cycles in 0.1 M $HClO_4$ solution (a); XRD patterns of np-Pd_1Cu_1 before and after electrochemical cycling (b).

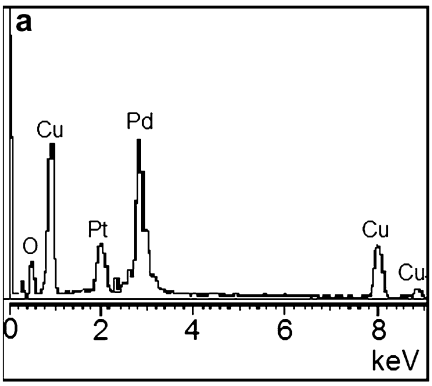

b	Element	Wt.%	At.%
Pt/Pd_3Cu_1	Pt	13.3	7.0
	Pd	72.4	69.9
	Cu	14.3	23.1
Pt/Pd_1Cu_1	Pt	14.2	6.8
	Pd	55.0	48.1
	Cu	30.8	45.1
Pt/Pd_3Cu_7	Pt	16.8	7.3
	Pd	34.3	27.4
	Cu	48.9	65.3

Fig. 4. EDS spectrum of Pt/np-Pd_1Cu_1 (a); element compositions of the three Pt/np-PdCu determined by EDS (b).

mentioning that the Pt content calculated from the H_{ads} charge is in good agreement with that calculated by the Cu-UPD charge, further confirming the near monolayer deposition of Pt. As shown in Fig. 5c, these Pt/np-PdCu show greatly improved EASA-specific kinetic activities than both Pt/np-Pd and Pt/C. The current density at 0.90 V on np-Pd_1Cu_1 ($\sim$1.17 mA cm^{-2}) is the highest one which is $\sim$5.8-fold that of Pt/C ($\sim$0.2 mA cm^{-2}). The order of the activities is Pt/np-Pd_1Cu_1 > Pt/np-Pd_3Cu_7 > Pt/np-Pd_3Cu_1 > Pt/np-Pd > Pt/C. The Pt mass-specific activity of Pt/np-Pd_1Cu_1 is $\sim$2.01 A mg^{-1} which is $\sim$9.5-fold that of Pt/C (0.21 A mg^{-1}). Since Pd is also a precious metal, the mass of Pd should also be included. The Pt + Pd mass activity of Pt/np-Pd_1Cu_1 is still $\sim$1.9-fold that of Pt/C. The enhanced utilization of Pd in the core by using PdCu alloy nanostructures not only improves the activity of the Pt shell but also makes the developed electrocatalyst more economical for practical applications.

Compared with Pt/C catalyst, the activity enhancement in Pt/np-Pd can be attributed to the unique core–shell structure, which modifies both the structural and electronic properties of the Pt monolayer. Specifically, the Pd substrate is believed to apply a compressive strain upon the Pt monolayer and also impart a so-called "ligand-effect" which would lower the energy of the Pt d-band center [18,42]. The lowered Pt d-band energy is thought to provide for a weakened interaction with oxygen-containing species, thereby yielding an improved ORR activity [24]. To explain the greatly improved activity of Pt/np-Pd_1Cu_1, it is known that the different Cu contents in the PdCu alloy core would have different strain effects on the Pd shell [43], which would further modifies the structural and electronic properties of the Pt monolayer. Since only moderately compressed Pt surface is most conducive for ORR [18], the np-Pd_1Cu_1 core probably results in a more suitably strained Pt monolayer shell. Moreover, density functional theory calculation has revealed that the incorporation of Cu in the Pd core can further lower the binding energy of oxygen-containing species on the deposited Pt monolayer compared with pure-Pd core due to effects from the compressive strain and electron redistribution between the PdCu core and Pt shell [17].

As mentioned above, the stability of electrocatalysts is vital for their practical applications. The stability of the Pt/np-PdCu, Pt/np-Pd and Pt/C were evaluated by continuous potential cycling

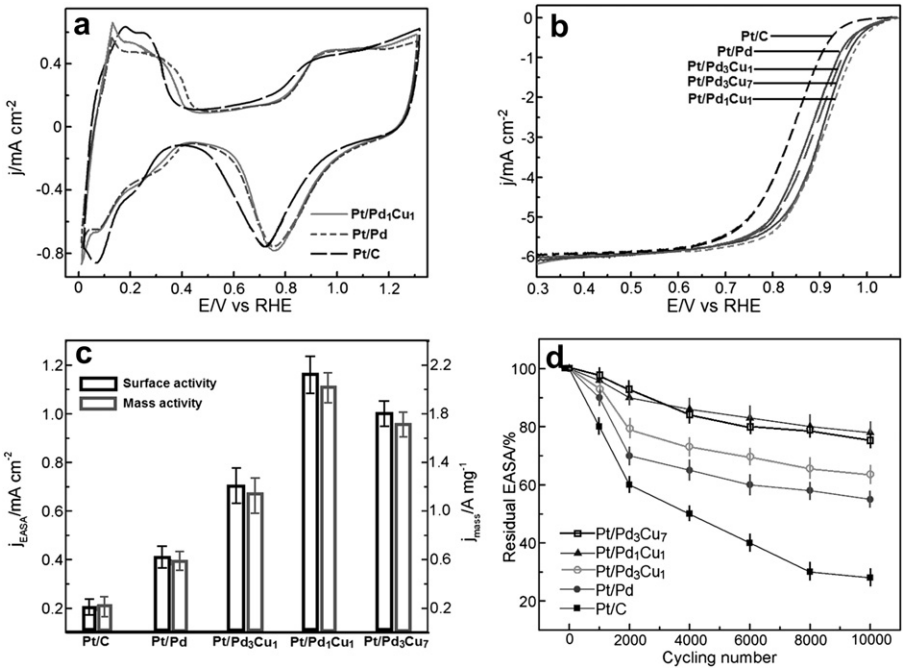

Fig. 5. CVs of Pt/np-Pd_1Cu_1, Pt/np-Pd and Pt/C in N_2-saturated 0.1 M $HClO_4$ solution (a); ORR polarization curves of the five catalysts in O_2-saturated 0.1 M $HClO_4$, obtained using a rotating disk electrode at 1600 rpm (b); surface and Pt mass-specific current densities of the five catalysts at 0.9 V (c); changes of EASAs of the five catalysts with increasing cycle numbers (0.6–1.2 V, scan rate: 50 mV s^{-1}) (d).

between 0.6 and 1.2 V in 0.1 M $HClO_4$ solution for 10,000 cycles. The EASAs of these catalysts decrease gradually with the increasing potential cycles (Fig. 5d). In comparison, the Pt/np-Pd_1Cu_1 and Pt/np-Pd_3Cu_7 show similar high stability. After 10,000 cycles, Pt/np-Pd_1Cu_1 remains ~78% of the original value, however, the EASA of Pt/np-Pd decreases to ~55% of the initial value. Under the same conditions, Pt/C catalyst undergoes ~72% loss in EASA. These results indicate that both the composition and structure of the core influence the stability of the Pt shell greatly. It is known that destabilization of Pt/C is associated with Ostwald ripening, aggregation of supported Pt nanoparticles and the loss of support contact due to carbon corrosion. Unlike Pt/C-like supported catalysts, the destabilization of supportless nanoporous metals is usually caused by coarsening of ligaments [44]. Since both Pt and Pd have very small surface diffusivity [45], the coarsening of Pt/Pd ligament is believed to be significantly retarded. The improved stability of Pt/np-Pd_1Cu_1 compared with those of Pt/np-Pd_3Cu_1 and Pt/np-Pd should be attributed to the uniquely strained Pt monolayer and underlayer Pd shell by the PdCu alloy core. Without the Pt monolayer, the improved stability of np-Pd_1Cu_1 compared with np-Pd under electrochemical cycling conditions has also been observed [40], which can be attributed to the increased dissolution potential for Pd on more active Cu [46].

4. Conclusions

np-PdCu near-surface alloys are successfully prepared by a two-step dealloying route. The Pt monolayer is then deposited on the np-PdCu near-surface alloy core by a Cu-UPD–Pt displacement strategy. We demonstrate that the Pt monolayer on np-Pd_1Cu_1 core shows the highest surface activity for ORR which is ~5.8-fold that of state-of-the-art Pt/C catalyst. The Pt/np-Pd_1Cu_1 also shows much enhanced stability compared with Pt/C. With improved ORR activity, stability and decreased noble metal loading, the Pt/np-Pd_1Cu_1 is very promising for practical applications.

Acknowledgement

This work is supported by the Scientific Innovation Team Project of Ningbo (2011B82014), K.C. Wong Education Foundation and K.C. Wong Magna Fund, Hong Kong.

Reference

[1] H.A. Gasteiger, N.M. Markovic, Science 324 (2009) 48.
[2] F. Fouda-Onana, S. Bah, O. Savadogo, J. Electroanal. Chem. 636 (2009) 1.
[3] I.J. Hsu, Y.C. Kimmel, Y. Dai, S. Chen, J.G. Chen, J. Power Sources 199 (2012) 46.
[4] F. Gobal, R. Arab, J. Electroanal. Chem. 647 (2010) 66.
[5] Z.Z. Jiang, Z.B. Wang, Y.Y. Chu, D.M. Gu, G.P. Yin, Energ. Environ. Sci. 4 (2011) 728.
[6] S. Koh, P. Strasser, J. Am. Chem. Soc. 129 (2007) 12624.
[7] T.Y. Jeon, S.J. Yoo, Y.H. Cho, S.H. Kang, Y.E. Sung, Electrochem. Commun. 12 (2010) 1796.
[8] J.R.C. Salgado, E. Antolini, E.R. Gonzalez, J. Power Sources 141 (2005) 13.
[9] K.C. Neyerlin, R. Srivastava, C. Yu, P. Strasser, J. Power Sources 186 (2009) 261.
[10] W. He, J. Liu, Y. Qiao, Z. Zou, X. Zhang, D.L. Akins, H. Yang, J. Power Sources 195 (2010) 1046.
[11] U.A. Paulus, A. Wokaun, G.G. Scherer, T.J. Schmidt, V. Stamenkovic, V. Radmilovic, N.M. Markovic, P.N. Ross, J. Phys. Chem. B 106 (2002) 4181.
[12] V.R. Stamenkovic, B.S. Mun, K.J.J. Mayrhofer, P.N. Ross, N.M. Markovic, J. Am. Chem. Soc. 128 (2006) 8813.
[13] J.A. Zhao, A. Manthiram, Appl. Catal. B 101 (2011) 660.
[14] T. Toda, H. Igarashi, M. Watanabe, J. Electroanal. Chem. 460 (1999) 258.
[15] E. Antolini, R.R. Passos, E.A. Ticianelli, Electrochim. Acta 48 (2002) 263.
[16] W. Chen, J.M. Kim, S.H. Sun, S.W. Chen, J. Phys. Chem. C 112 (2008) 3891.
[17] M. Shao, K. Shoemaker, A. Peles, K. Kaneko, L. Protsailo, J. Am. Chem. Soc. 132 (2010) 9253.
[18] J.X. Wang, H. Inada, R.R. Adzic, J. Am. Chem. Soc. 131 (2009) 17298.
[19] J.H. Jang, J. Kim, Y.H. Lee, I.Y. Kim, M.H. Park, C.W. Yang, S.J. Hwang, Y.U. Kwon, Energ. Environ. Sci. 4 (2011) 4947.
[20] P. Mani, R. Srivastava, P. Strasser, J. Phys. Chem. C 112 (2008) 2770.
[21] A. Sarkar, A.V. Murugan, A. Manthiram, Langmuir 26 (2010) 2894.
[22] A. Sarkar, A. Manthiram, J. Phys. Chem. C 114 (2010) 4725.
[23] L. Xiong, A. Manthiram, Electrochim. Acta 50 (2005) 2323.
[24] J.L. Zhang, M.B. Vukmirovic, Y. Xu, M. Mavrikakis, R.R. Adzic, Angew. Chem. Int. Ed. 44 (2005) 2132.
[25] N. Hoshi, M. Nakamura, S. Kondo, Electrochem. Commun. 11 (2009) 2282.
[26] S. Song, Y. Wang, P.K. Shen, J. Power Sources 170 (2007) 46.
[27] K.H. Lee, K. Kwon, V. Roev, D.Y. Yoo, H. Chang, D. Seung, J. Power Sources 185 (2008) 871.
[28] M.H. Lee, J.S. Do, J. Power Sources 188 (2009) 353.
[29] R.-F. Wang, S.-J. Liao, H.-Y. Liu, H. Meng, J. Power Sources 171 (2007) 471.
[30] H. Gharibi, R.A. Mirzaie, E. Shams, M. Zhiani, M. Khairmand, J. Power Sources 139 (2005) 61.
[31] Z.W. Chen, M. Waje, W.Z. Li, Y.S. Yan, Angew. Chem. Int. Ed. 46 (2007) 4060.
[32] S.H. Sun, G.X. Zhang, D.S. Geng, Y.G. Chen, R.Y. Li, M. Cai, X.L. Sun, Angew. Chem. Int. Ed. 50 (2011) 422.
[33] Y.M. Tan, J.M. Fan, G.X. Chen, N.F. Zheng, Q.J. Xie, Chem. Commun. 47 (2011) 11624.
[34] Z. Zhang, Y. Wang, Z. Qi, W. Zhang, J. Qin, J. Frenzel, J. Phys. Chem. C 113 (2009) 12629.
[35] Y. Ding, M.W. Chen, J. Erlebacher, J. Am. Chem. Soc. 126 (2004) 6876.
[36] L.Y. Chen, H. Guo, T. Fujita, A. Hirata, W. Zhang, A. Inoue, M.W. Chen, Adv. Funct. Mater. 21 (2011) 4364.
[37] L.F. Liu, E. Pippel, R. Scholz, U. Gosele, Nano Lett. 9 (2009) 4352.
[38] X.G. Wang, H. Ji, Z.H. Zhang, Electrochem. Commun. 11 (2009) 1896.
[39] C. Xu, Y. Liu, J. Wang, H. Geng, H. Qiu, J. Power Sources 199 (2012) 124.
[40] C.X. Xu, A.H. Liu, H.J. Qiu, Electrochem. Commun. 13 (2011) 766.
[41] H.A. Gasteiger, S.S. Kocha, B. Sompalli, F.T. Wagner, Appl. Catal. B 56 (2005) 9.
[42] C. Koenigsmann, A.C. Santulli, S.S. Wong, R.R. Adzic, J. Am. Chem. Soc. 133 (2011) 9783.
[43] P. Strasser, S. Koh, T. Anniyev, J. Greeley, K. More, C.F. Yu, Z.C. Liu, S. Kaya, D. Nordlund, H. Ogasawara, M.F. Toney, A. Nilsson, Nat. Chem. 2 (2010) 454.
[44] X.Y. Lang, H. Guo, L.Y. Chen, M.W. Chen, J. Phys. Chem. C 114 (2010) 2600.
[45] J. Erlebacher, J. Electrochem. Soc. 151 (2004) C614.
[46] J. Greeley, J.K. Nørskov, Electrochim. Acta 52 (2007) 5829.